Earth System
Dynamics
Discussions

EGU

Multi-million year cycles in modelled $\delta^{13}C$ as a response to astronomical forcing of organic matter fluxes.

Gaëlle Leloup[1,2] and Didier Paillard[2]

[1]Agence Nationale pour la gestion des déchets radioactifs (ANDRA), 1 Rue Jean Monnet, 92290 Châtenay-Malabry, France
[2]Laboratoire des Sciences du Climat et de l'Environnement, LSCE/IPSL, CEA-CNRS-UVSQ-Université Paris-Saclay, 91198 Gif-sur-Yvette, France

Correspondence: Gaëlle Leloup (gaelle.leloup@lsce.ipsl.fr)

Abstract.

Along with 400 kyr periodicities, multi-million year cycles have been found in $\delta^{13}C$ records over different time periods. A ∼8-9 Myr periodicity is found throughout the Cenozoic, and part of the Mesozoic. The robust presence of this periodicity in $\delta^{13}C$ records suggests an astronomical origin. However, this periodicity is barely visible in the astronomical forcing. Due

5   to the large fractionation factor of organic matter, its burial or oxidation produces large $\delta^{13}C$ variations for moderate carbon variations. Therefore, astronomical forcing of organic matter fluxes is a plausible candidate to explain the oscillations observed in the $\delta^{13}C$ records. So far, modelling studies forcing astronomically the organic matter burial have been able to produce 400 kyr and 2.4 Myr cycles in $\delta^{13}C$, but were not able to produce longer cycles, such as 8-9 Myr cycles. Here, we propose a mechanism that could explain the presence of multi-million year cycles in the $\delta^{13}C$ records, and their stability over time, as

10   a result of preferential periodicity locking to multiples of astronomical forcing periods. With a simple non linear conceptual model for the carbon cycle that has multiple equilibria, we are able to extract longer periods than with a simple linear model, and more specifically, multi-million year periods.

1 Introduction

Astronomical frequencies are imprinted into the carbon cycle. A 400 kyr oscillation has been seen in many $\delta^{13}C$ records

15   covering the Cenozoic : during the Paleocene (Westerhold et al., 2011), the Eocene (Lauretano et al., 2015), the Oligocene (Pälike et al., 2006), Miocene (Billups et al., 2004) and during more recent time periods (Wang et al., 2010). The 400 kyr frequency corresponds to one of the frequencies of eccentricity, and this is the most stable astronomical periodicity through geological times (Laskar, J. et al., 2004).

Longer cycles of 2.4 Myr have also been found in $\delta^{13}C$ records over the Cenozoic : over the Oligocene (Pälike et al., 2006;

20   Boulila et al., 2012), and Miocene (Liebrand et al., 2016). The 2.4 Myr periodicity is at the same time a true eccentricity cycle and present in the amplitude modulation (AM) of the 100 kyr and 400 kyr cycles (Laskar, J. et al., 2011; Boulila et al., 2012). ∼4.5 Myr cycles have also been observed in $\delta^{13}C$ in the late Creataceous (Sprovieri et al., 2013) as well as the latest Ordovician and Silurian (Sproson, 2020).

Much longer and dominant cycles of approximately 9 Myr have been found in $\delta^{13}C$ records, over the Cenozoic (Boulila et al.,

25   2012) and the Mesozoic (Martinez and Dera, 2015). Cycles of around 8 Myr have been seen in $\delta^{13}C$ in the late Creataceous
(Sprovieri et al., 2013). This periodicity therefore seems very stable over time. The robust presence of $\sim$9 Myr cycles over
various time periods, hints at an astronomical origin. However, in the case of 4.5 Myr and 9 Myr cycles, the link to the
astronomical forcing is less clear, as these frequencies are not easily seen in the eccentricity spectra. A $\sim$4.5 Myr periodicity
is visible in the eccentricity solution, although with a very low amplitude. The AM envelopes of the 100 kyr and 400 kyr

30   eccentricity also show a $\sim$4.5 Myr cyclicity, but again with low amplitude. The $\sim$9 Myr frequency is not directly visible in the
eccentricity spectra. Although it has been suggested that the AM envelope of the $\sim$2.4 Myr filtered eccentricity has a $\sim$9 Myr
cyclicity (Boulila et al., 2012), this remains with a very low amplitude. Therefore, the way in which the astronomy could pace
these multi-million year cycles remains mysterious.

It has been suggested (Paillard, 2017; Kocken et al., 2019) that an astronomical forcing of organic carbon fluxes could explain

35   the observed $\delta^{13}C$ cyclicities at 400 kyr and 2.4 Myr. Indeed, organic, ^{12}C enriched, matter burial or oxidation can lead
to relatively large δ^{13}C variation for a moderate carbon variation, which is not possible with silicate weathering (Paillard,
2017; Russon et al., 2010). It is usually assumed that long term carbon cycle is mainly controlled by silicate weathering. But
it is a negative feedback, that does not allow for oscillatory behaviour as observed in the data. Additionally, recent studies
have highlighted the importance played by organic carbon fluxes in the long term carbon budget, acting as either a source if

40   petrogenic organic carbon is eroded and oxidized, or a sink if terrestrial organic carbon is exported and buried into sediments
(Hilton and West, 2020). Organic carbon contributions are of the same order of magnitude than silicate weathering (Hilton and
West, 2020). Therefore, astronomical forcing of the organic matter burial is a plausible candidate to explain the observed cyclic
$\delta^{13}C$ variations.

Kocken et al. (2019) suggested that the link between $\delta^{13}C$ and the astronomical forcing could be explained by enhanced marine

45   organic carbon burial for lower eccentricity values. Periods of low eccentricity and therefore low seasonal contrast could favor
annual wet conditions, and consequently clay formation. The majority of organic carbon burial is buried in association with
clay particles (Hedges and Keil, 1995). If transport is not limiting, lower eccentricity would lead to higher marine organic
carbon burial and increase $\delta^{13}C$. Paillard (2017) suggested a link between monsoons and organic carbon burial. Monsoon
favor soil erosion and sediment transports. Recent soil as well as petrogenic organic carbon can be eroded and carried to

50   the oceans via rivers. The net effect on organic carbon burial depends on the geomorphological dynamics. For aggradational
situations, that favour burial, the net result is organic matter burial. In that case, $\delta^{13}C$ increases with increased eccentricity and
monsoon strength. However, for progradational situations, oxidation of petrogenic organic carbon is favoured, leading to a $\delta^{13}C$
decrease with eccentricity increase. Martinez and Dera (2015) suggested that low eccentricity values and the associated stable
and humid conditions could favor constant freshwater and nutrient inputs, thus favoring water mass stratification, productivity

55   levels, leading to persistent anoxia and therefore higher organic carbon burial rates. On the contrary, high eccentricity values are
associated with a recovery of oxic conditions during the cool season, limiting organic carbon burial. It has also been suggested
that terrestrial organic carbon burial could increase with eccentricity minima, as this would favor annual soil anoxia (Kurtz
et al., 2003). Laurin et al. (2015) suggested that $\delta^{13}C$ variations in the Late Cretaceous could be explained by a transient
storage of organic matter or methane in quasi-stable reservoirs such as wetlands, soils, marginal zones of marine euxinic strata,

60 and permafrost. These quasi-stable reservoirs could respond non linearly to changes in obliquity and the consequent high latitude insolation changes or changes in meriodional insolation gradients. Other mechanisms have been proposed to explain $\delta^{13}C$ variation as a consequence from astronomical variations. de Boer et al. (2014) suggested that ice sheet dynamics and linked changes in carbon cycle dynamics could explain the 400 kyr cycles in $\delta^{13}C$. However, this mechanism does not permit to explain the presence of such cycles for periods without ice sheet (Kocken et al., 2019).

65 Modelling studies forcing the net organic matter burial through eccentricity have been able to produce 400 kyr and 2.4 Myr cycles in the $\delta^{13}C$ (Paillard, 2017; Kocken et al., 2019). However, these studies did not find longer cycles, such as the $\sim$4.5 and $\sim$9 Myr cycles observed in geological records. The model used were linear, and non linear mechanisms might be necessary in order to produce multi-million year cycles that have a very low amplitude in the input forcing.

Here, we develop a new conceptual model of the carbon cycle, that includes a net organic matter burial term and force it 70 astronomically with the eccentricity, similarly to the study of Paillard (2017). However, contrary to this study, the organic matter fluxes depend also on the surface carbon content, through its influence on climate, and on atmospheric oxygen content. Our model therefore couples the carbon and oxygen cycle, and is non linear, with the possibility of multiple equilibria. With this model, it is possible to obtain multi-million year frequencies in the $\delta^{13}C$. Depending on the strength of the astronomical forcing, periodicities of 2.4 Myr, $\sim$4.8 Myr $\sim$7 Myr, and $\sim$9 Myr are produced preferentially, presumably as a result of 75 periodicity doubling of the 2.4 Myr eccentricity frequency.

2 Methods

2.1 Model description

Here, we develop a simple, yet non linear conceptual model, coupling the carbon and oxygen cycle. When forced by the eccentricity signal as input, the model is able to produce multi-million year frequencies as output, and multiples of the 2.4 Myr 80 frequency of eccentricity : 2.4 Myr cycles, $\sim$4.5 Myr cycles, $\sim$7 Myr cycles and $\sim$9 Myr cycles.

Our model is based on the conceptual model of Paillard (2017). This model represents the evolution of the surface Earth carbon content, including the atmosphere, the ocean and the biosphere. This is opposed to carbon stored in deep soils, rocks or sediments. In our model, we have added a crude representation of the surface oxygen evolution. In the following, the features common to the Paillard (2017) model and ours are summarized and the differences are described.

85 In our model, the modeling of the surface carbon evolution is identical to the Paillard (2017) model. The surface carbon evolution is determined by the volcanic input V, the oceanic carbonate deposition flux D that is associated with silicate weathering, and the organic carbon burial B.

$$\frac{dC}{dt} = V - B - D \tag{1}$$

The organic matter burial B is meant as a net burial, and represents all organic carbon fluxes. $B = B^+ - B^-$ where B^+ 90 represents organic carbon burial and B^- represents organic matter oxidation.

As in Paillard (2017), we assume that the oceanic calcium concentration does not vary significantly over time and that carbonate compensation restores the oceanic carbonate content. With the use of an alkalinity balance (see Paillard (2017) for details), we obtain the following equation for the carbon evolution :

$$\frac{dC}{dt} = 2(V - B) - W \tag{2}$$

95   where W is the alkalinity flux to the ocean associated with silicate weathering. As in Paillard (2017), we assume silicate weathering to be the main stabilizer of the carbon system, with a fixed relaxation time τ_c : W = C/τ_c. The volcanic input is considered as constant, $V = V_0$. The $\delta^{13}C$ evolution is described by :

$$\frac{d\delta^{13}C}{dt} = \frac{1}{C}(V(\delta^{13}V - \delta^{13}C) - B(\delta^{13}B - \delta^{13}C)) \tag{3}$$

We have assumed a constant -5‰ volcanic source ($\delta^{13}V$ = -5‰) and a constant -25‰ organic matter fractionnation ($\delta^{13}B -$
100   $\delta^{13}C$ = -25‰). This slightly differs from the equation used in Paillard (2017), however the results remain very similar (for a detailed discussion, see the interactive discussion of the Paillard (2017) paper).

Compared to the previous model, we have added a crude representation of the oxygen cycle. Indeed, the oxygen interacts closely with organic matter burial and oxidation. On one side, the burial of organic matter is facilitated in low oxygen zones. On the other side, organic matter oxidation reduces the oxygen quantity, while burial of organic matter adds oxygen to the
105   surface system. We consider a global oxygen content O, representing both the atmospheric O_2 and dissolved O_2 in oceans. On geological timescales, the atmospheric O_2 is driven by the net organic matter burial, the net burial of pyrite ($F_{pb} - F_{po}$ with F_{pb} and F_{po} the pyrite burial and oxidation), oxidation of volcanic gases (F_v) and oxidative weathering of sedimentary rocks, not already accounted in the net organic matter and pyrite burial, such as ferrous iron (F_w) (Berner, 2001; Canfield, 2005).

$$\frac{dO}{dt} = (B^+ - B^-) + (F_{pb} - F_{po}) - F_v - F_w \tag{4}$$

110   The oxidation of other elements than organic carbon is grouped in a single term, Ox, leading to :

$$\frac{dO}{dt} = B - Ox \tag{5}$$

We make the assumption that the oxidation of other elements than organic carbon increases linearly with oxygen contents : $Ox = a_{ox} \cdot O + b_{ox}$, with a_{ox} and b_{ox} two constants.

Although organic carbon perturbations are expected to have a weak impact on atmospheric O_2 concentrations, as atmospheric
115   O_2 is relatively high in the Phanerozoic (Bergman et al., 2004; Berner and Canfield, 1989), perturbations to atmospheric O_2 of a few permill have been seen in Pleistocene ice cores (Stolper et al., 2016).

As in the Paillard model, the organic matter burial is forced astronomically, while the forcing term differs slightly in both models. Here, we choose to express the organic matter burial variations as :

$$B = B_0 - a_f F(t)$$

120   with F(t) = (e(t) -mean(e(t))) / max(e(t)) where e(t) is the eccentricity at time t, mean and max represent respectively the mean and maximum of eccentricity over the time period considered. B_0 represents the organic matter burial value without

astronomical forcing. The Analyseries software (Paillard et al., 1996) provides the La04 orbital parameters (Laskar, J. et al., 2004).

Several mechanisms have been proposed to be responsible of the link between organic matter burial and astronomical forcing.
125 Here, we do not intend to focus on a specific mechanism. We rather focus on the output signal that can be obtained from a simple astronomical forcing. Therefore, we have chosen the easiest possible relationship : a linear variation of the organic matter burial with the astronomical forcing. The negative sign was chosen in order to match the data, where eccentricity minima correspond to $\delta^{13}C$ minima, and thus organic matter burial maxima.

In the Paillard model, the B_0 term was constant and the organic matter burial therefore only varried with the astronomical
130 forcing. However, in our model, the organic matter burial depends not only on the astronomical forcing but also on the surface carbon content and the oxygen content, meaning $B_0 = B_0(C,O)$, as explained below.

Organic matter burial is facilitated in locally lower oxygen concentrations. All other things being equal, a higher oxygen content globally in the atmosphere will lead to higher oxygen contents locally in the ocean. Therefore, organic matter burial decreases for higher oxygen concentrations and inversely. Here, we have assumed an inverse linear dependency between the
135 organic matter burial and the oxygen content O. If O_1 and O_2 are two oxygen contents, then the difference in organic matter burial (for the same carbon content C) is :

$$B_0(C,O_1) = B_0(C,O_2) - \delta(O_1 - O_2) \tag{6}$$

δ is a positive constant. For a similar carbon content C, the organic matter burial is higher in the case of lower oxygen quantities.

140 Here, we also suggest that net organic carbon burial depends on the surface carbon quantity C. Indeed, climate can influence the organic matter burial, and as a first approximation, larger carbon values C in the surface system correspond to warmer, wetter climates. Net organic matter burial contribution to the surface carbon evolution is composed of two opposite contributions : biospheric organic carbon erosion leading to CO_2 drawdown (CO_2 sink) and therefore surface carbon decrease, and oxidation of petrogenic organic carbon, leading to CO_2 rise (CO_2 source), and therefore surface carbon increase. Eroded terrestrial
145 organic matter from plants is delivered to rivers (Meybeck, 1982; Ludwig et al., 1996). If a part of this biospheric organic carbon is buried into sediments without being degraded, this corresponds to a decrease of the surface carbon content. It has been estimated that the current burial flux of organic carbon eroded from land into oceanic sediments is around 40-80 MtC/yr (Hilton and West, 2020). On the other hand, exhumation of sedimentary rocks can lead to the oxidation of petrogenic organic carbon and therefore to CO_2 release (Hilton et al., 2014). The carbon flux released to the atmosphere through petrogenic or-
150 ganic carbon oxidation has been estimated to be between 40 and 100 MtC/yr (Hilton and West, 2020). Climate can act on these processes on several ways. When the surface carbon content increases, this globally results in a warmer and wetter climate. Warmer temperatures and stronger runoff increase erosion and transfer of biospheric organic carbon (Hilton, 2017; Smith et al., 2013). In addition, warmer temperatures increase ocean stratification and decrease the solubility of oxygen in surface waters (Bopp et al., 2002), leading to expansion of oxygen minimum zones (Stramma et al., 2008, 2010). This decreases organic
155 matter oxidation and favours its burial into oceanic sediments (Jessen et al., 2017). Other climatic related factors, have been

suggested to limit dissolved oxygen in the ocean, such as increased phosphorus inputs (Baroni et al., 2020; Niemeyer et al., 2017). These inputs are expected to increase for warmer and wetter climate, that increases weathering, leading to regional deoxygenation and organic carbon burial (Baroni et al., 2020).

It has also been suggested that the oxidation of petrogenic organic carbon could be linked to climate as petrogenic organic car-
160 bon oxidation could be locally limited by temperature, O_2 contents, and microbial activity (Chang and Berner, 1999; Bolton et al., 2006; Hemingway et al., 2018; Petsch et al., 2005). Higher temperature could lead to stronger petrogenic carbon oxidation. We have made the assumption that for intermediate carbon value, and thus intermediate temperatures, this mechanism is dominant, whereas the increase in export of biospheric carbon and increased burial dominates for warmer temperatures (larger C values). We have supposed that there is no dependency to climate for lower carbon values. This results in a non monotonic
165 dependency of B to C. For low carbon values (C $<C_1$) and thus colder climates, the organic carbon burial B does not depend on C. Then, for intermediate carbon values ($C_1 < $ C $ < C_2$), the organic carbon burial decreases with increasing temperatures, and thus increasing carbon C. Finally, for higher carbon values (C $> C_2$) the organic carbon burial increases with increasing temperature (and thus, carbon C). For the sake of simplicity, we have made the assumption of linear variations. The resulting shape of the evolution of organic carbon burial fluxes as function of the carbon content C is represented in Figure 1.
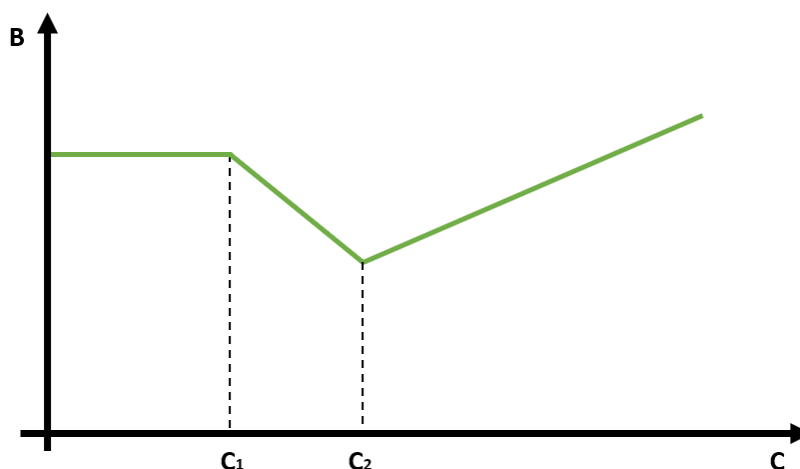
Figure 1. Schematic representation of the organic carbon burial B evolution with carbon content C

170   These assumptions on the dependency of the organic matter burial flux to the surface carbon content C are strong. It is not an easy task to quantify at present day the net magnitude of carbon burial, as some regions are known to be carbon sinks and others known to be carbon sources. It is an even more complicated task to have an estimation of this budget for different climates, and therefore different carbon contents. However, the results discussed below do not depend on the specific shape chosen for the dependency of the organic matter burial B to the carbon content C. Similar results could be obtained with an other dependency,
175 as long as it is non monotonic with the carbon content C and we place ourselves here in one of the simplest case possible. The shape of the organic burial evolution is certainly different and more complex than the one presented here. However, as many

process act on the net organic matter burial, some favoring organic matter burial, and some favoring organic matter oxidation, we are confident in the fact that the relationship between organic matter burial and surface carbon content is non monotonic. In our model, carbon and oxygen evolution depend on the organic matter burial term, that conversely depends on both, carbon

180 and oxygen quantities. Therefore, in our model the carbon and oxygen cycle are coupled via the organic matter burial term. This is the main difference with the model of Paillard 2017, as this results in a non linear model, where it is possible to have multiple equilibria in the carbon and oxygen system, and thus oscillations even without astronomical forcing.

2.2 Parameter values

We first consider the case where the organic matter burial is not forced astronomically ($a_f = 0$). For simplicity, we have chosen

185 B_0 to be piecewise constant when considering the variations due to carbon. It is decreasing linearly with oxygen. Therefore, we can write B_0 as :

$$B_0(C,O) = B_0(C,O_{ref}) - \delta(O - O_{ref}) \tag{7}$$

with

$$B_0(C,O_{ref}) = \begin{cases} \alpha & \text{for C} < C_1 \\ \alpha - \beta(C - C_1) & \text{for } C_1 < \text{C} < C_2 \\ \alpha - \beta(C_2 - C_1) + \gamma(C_2 - C_1) & \text{for C} > C_2 \end{cases} \tag{8}$$

190 Where δ ($\delta > 0$) is the coefficient representing the strength of the organic matter burial evolution with oxygen. The higher δ, the stronger is the organic matter burial decrease with oxygen content. α represents the constant value of organic matter burial for low carbon values ($C < C_1$). $-\beta$ ($-\beta < 0$) represents the slope of the carbon burial evolution for intermediate carbon values ($C_1 < C < C_2$), for which the organic matter burial decreases with increasing carbon content. γ ($\gamma > 0$) represents the slope of the carbon burial evolution for high carbon values ($C > C_2$), for which the organic matter burial increases with increasing

195 carbon content. We choose to place ourselves in the case where there are two stable equilibria for the carbon cycle for the current oxygen value (see section 3.1). This corresponds to panel (a) of Figure 2. These equilibria are called C_{eq1ref} and C_{eq2ref}.

Our unforced model therefore contains 13 parameters : the value of carbon emissions associated with volcanism V_0, the time constant associated with silicate weathering τ_c, the current oxygen content O_{ref}, the two values of the equilibria for $O = O_{ref}$,

200 C_{eq1ref} and C_{eq2ref}, parameters linked to the shape of the evolution of organic carbon burial with carbon (C_1, C_2, β, γ, α), one parameter linked to the evolution of organic matter burial with oxygen (δ), and two parameters linked to the evolution of oxidation of other elements than carbon with oxygen (a_{ox} and b_{ox}). When the organic carbon burial is forced astronomically, there is one additional parameter, representing the strength of the astronomical forcing : a_f.

O_{ref} is the current oxygen level and is equal to $O_{ref} = 1.19 \cdot 10^6$ Pg. C_{eq1ref} and C_{eq2ref} are the stable equilibria for

205 $O = O_{ref}$. We have choosen C_{eq1ref} to be equal to the pre industrial carbon content of Earth's surface reservoirs (atmosphere, oceans and biosphere). It is estimated to be around 43 000 PgC (Ciais et al., 2013). We have chosen the second equilibria to be

at higher carbon values, C_{eq2ref} = 47000 PgC. The τ_c constant is set to 200 kyr (Archer et al., 1997). The V_0 value was chosen in order to have $\delta^{13}C$ values around zero for medium carbon values, $V_0 = (5/8) \cdot (1/2)(C_{eq1ref} + C_{eq2ref})/\tau_c$ = 140 TgCyr^{-1}. This is a value slightly higher than in Paillard (2017). However, it remains in the range of possible values for carbon emissions

210   from volcanism, estimated between 40 and 175 TgC/yr (Burton et al., 2013). That C_{eq1ref} and C_{eq2ref} are equilibria for $O = O_{ref}$ in the unforced case gives constraints on the α and γ parameters. Several values of β remain possible, with the constraint that we should have $\beta > 1/2\tau_c$. C_1 and C_2 should be contained between C_{eq1ref} and C_{eq2ref} : $C_{eq1ref} < C_1 < C_2 < C_{eq2ref}$. In the following, we have taken $\beta = 2.4 \cdot 1/2\tau_c$, $C_1 = C_{eq1ref} + (1/3)(C_{eq2ref} - C_{eq1ref})$, $C_2 = C_{eq1ref} + (2/3)(C_{eq2ref} - C_{eq1ref})$. Changing these parameters would change slighlty the form of the unforced oscillations. The δ parameter influences

215   the size of the free oscillations for the oxygen. We have set δ in order to have free oscillations of the size of a few percent of the reference oxygen value. This corresponds to $\delta \sim 2 \cdot 10^{-7}$. Different values of the parameters a_{ox} and b_{ox} are studied in the following, corresponding to the four possible different cases outlined by the four panels of Figure 3 (see Section 3.1).

3   Results and discussion

Here we study the results for three different cases to examine the importance of the different processes.

220   – In a first step, we do not consider astronomical variations of the organic matter burial B. Therefore, organic matter burial only depends on the carbon and oxygen quantities, $B = B_0(C,O)$.

– In a second step, we consider a formulation similar to the model of Paillard (2017), where the organic matter burial depends on the astronomical forcing but does not depend on the carbon and oxygen quantities : $B = B_{0cst} - a_f F(t)$ with B_{0cst} being a constant.

225   – In a last step, we consider that the organic matter burial depends on both the astronomical forcing and the carbon and oxygen contents (complete form) : $B = B_0(C,O) - a_f F(t)$

3.1   Results without astronomical forcing of the organic matter burial

First, we look at our model results in the case where the organic matter burial is not forced astronomically, corresponding to $a_f = 0 : B = B_0(C(t),O(t))$. This is done in order to better understand the dynamics of the coupled oxygen/ carbon system

230   without astronomical forcing. We first consider the system from a theoretical point of view, by describing the different possible equilibria. Then, we compute the results numerically for different parameter values.

Equilibria for the carbon are defined as $\frac{dC}{dt} = 0$. From equation 2, we get :

$$\frac{1}{2}\frac{dC}{dt} = (V - \frac{W}{2}) - B \tag{9}$$

Carbon equilibria are thus equivalent to $B = V - W/2$. As we have assumed $W = C/\tau_c$, and V to be constant, $V = V_0$, this

235   corresponds to $B = V_0 - C/(2\tau_c)$. Figure 2 represents schematically the evolution the organic matter burial term and the V - W/2 term as a function of the carbon content C. Depending on the relative position of the B curve to the V - W/2 curve, this

leads to one or two stable equilibria. For clarity, in the following we will call the B curve (green in the Figures) the organic term, and the V - W/2 curve (red curve) the inorganic term.
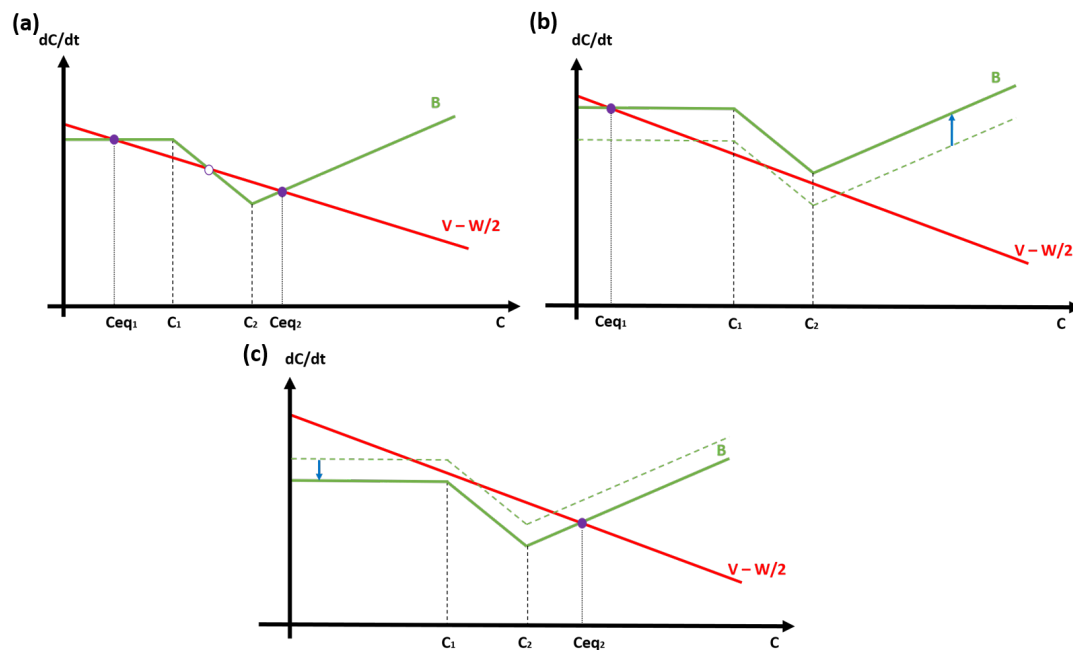
Figure 2. Schematic representation of the organic (green, B) and inorganic (red, $V_0 - C/(2\tau_c)$) terms as a function of the carbon content C. (a) Case of two equilibria in the carbon system (C_{eq1} and C_{eq2}). (b) Case of one equilibria in the carbon system, at low carbon value (C_{eq1}). (c) Case of one equilibria in the carbon system, at high carbon value C_{eq2}.

240   In the case represented by panel (a) of Figure 2, the organic and inorganic curves cross at three different locations, meaning that there are three different carbon values C for which an equilibrium is obtained ($dC/dt = 0$). However, only two of these equilibria are stable and are indicated by full purple circle, while the unstable equilibria is indicated by an empty purple circle. In the case of the empty circle, if we diverge a little from the equilibria value to higher carbon values, then V - W/2 > B (the red curve is above the green one) and thus dC/dt >0. This small divergence to higher carbon value, leads to even higher carbon values : the equilibrium is unstable. The same reasoning can be done if we diverge a little from the equilibrium towards lower

245   carbon values. On the contrary, if we consider the first full purple point from panel (a) of Figure 2, it is a stable equilibrium. If we diverge a little from this equilibrium towards higher carbon values, then B > V - W/2 (the green curve is above the red) and thus dC/dt < 0. The system is brought back towards lower carbon values : the equilibrium is stable. Panel (a) of Figure 2 represents the case of two stable equilibria in the carbon system. However, it is possible to have only one stable equilibrium in the carbon system, if the value of B is higher or lower, as is shown in panels (b) and (c) of Figure 2. In the

250   case of a higher organic matter burial, there is only one crossing between the green and red curves as represented in panel (b) of Figure 2 : there is only one equilibrium for the carbon cycle, C_{eq1}. A similar reasoning than previously shows that this

equilibrium is stable. In a similar manner, in the case of a lower organic matter burial, there is only one crossing between the green and red curves as represented in panel (c) of Figure 2 : there is only one equilibrium for the carbon cycle, C_{eq2}. This equilibrium is stable. These three configuration of the organic matter burial correspond to different oxygen values. Indeed, as

255   $B(C,O) = B(C,O_{ref}) - \delta(O - O_{ref})$, higher oxygen values correspond to a shift of the organic matter (green) curve towards the bottom, and conversely. Therefore, it is possible to switch between the configurations, if the oxygen evolves.

Similarly to what has been done for the carbon cycle, we look at possible equilibria in the oxygen cycle. In our model, dO/dt = 0 corresponds to $B = Ox$, meaning that the organic matter burial is equal to the oxidation of other elements than carbon. These terms are represented in Figure 3. The four different configurations shown in panels (a) - (d) correspond to different values for

260   the slope and intercept of the Ox curve. For these four configurations, the shape of the organic matter burial B (green) curve is similar. For low oxygen values ($O < O_{lim2}$), there is only one possible value of the organic matter burial B for each oxygen value. This corresponds to the case displayed in panel (b) of Figure 2, where there is only one possible equilibrium value for the carbon content C, and therefore only one possible value of B for a given oxygen value. For decreasing oxygen value, the organic burial increases. For high oxygen values, ($O > O_{lim1}$), there is also only one possible value of the organic matter burial

265   B for each oxygen value. This corresponds to the case displayed in panel (c) of Figure 2. There is only one possible value for the carbon content C, and therefore only one possible value of B for a given oxygen value. These values of organic carbon burial B are lower than the one obtained with $O < O_{lim2}$. For intermediate oxygen values ($O_{lim2} < O < O_{lim1}$) there are two possible equilibrium values for the carbon content C, and therefore two possible equilibrium values for the organic matter burial B for a given oxygen value. This corresponds to the case displayed in panel (a) of Figure 2. The unstable equilibrium is

270   displayed with dotted line.

Following our hypothesis, the Ox curve is simply a straight line. However, depending on the slope and intercept of the Ox curve, this leads to four different configurations, where the (blue) Ox curve either crosses the upper branch of B, the lower branch of B, none of them or both of them. These four different possibilities are schematized in Figure 3. When the Ox curve crosses the upper branch of B (Panel (b) of Figure 3), there is one possible equilibrium value for the oxygen (dO/dt = 0),

275   represented by the full orange circle. It is a stable equilibrium : if we divert to lower oxygen values, then B > Ox (the green curve is above the blue line), meaning that dO/dt > O, and the oxygen value increases back towards equilibrium. Similarly, when the Ox curve crosses the lower branch of B (Panel (c) of Figure 3), there is one possible equilibrium value for the oxygen. This is also a stable equilibrium. When the Ox curve crosses both the upper and lower branches of B (Panel (d) of Figure 3), it crosses also the middle, unstable, branch. There are three possible equilibrium values for the oxygen, two of which are stable

280   (the crossing with the upper and lower branch). For these three cases (panels (b), (c) and (d) of Figure 3), the system will converge towards an equilibrium value (C_{eq}, O_{eq}) and remain in this state as this are stable equilibria. When the equilibrium is reached the carbon and oxygen content will not evolve anymore. The organic matter burial and the $\delta^{13}C$ will therefore also not change.

However, the situation is different in the case where the Ox curve does not cross the lower or upper branch of B, but crosses

285   the middle branch (dashed line), as represented in Panel (a) of Figure 3. This branch is not stable from the carbon point of view (it corresponds to the unstable equilibria of Figure 2). It is also not a stable equilibria for oxygen. In this case, no equilibrium is
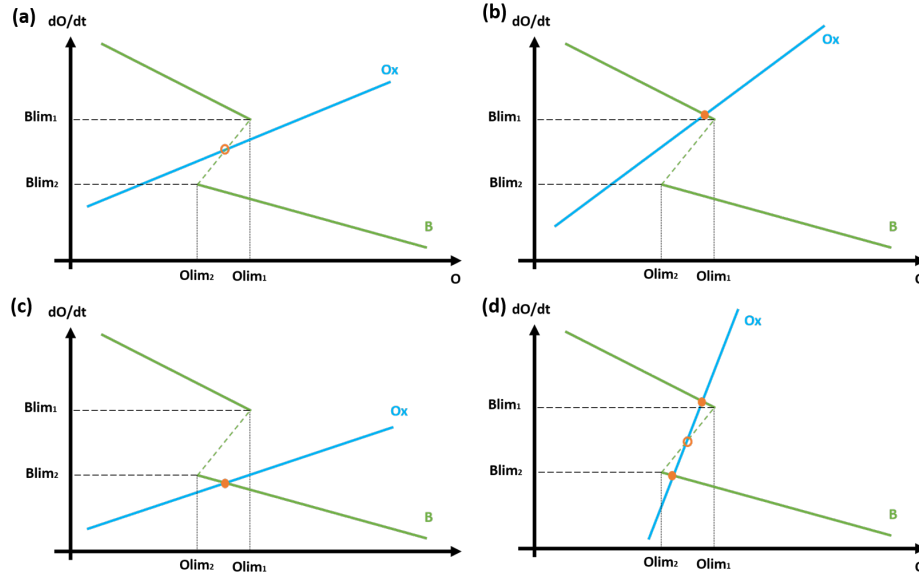
Figure 3. Schematic representation of the organic term (B, green curve) and the Ox term (blue curve) as a function of the oxygen content O. Four different cases are displayed, depending on the slope and intercept of the Ox curve : (a) one unstable equilibrium; (b) and (c) a stable equilibria; and (d) two stable equilibria

reached for the (C, O) system, and oscillations of the oxygen and carbon content can be obtained without astronomical forcing of the organic matter burial. The organic matter burial and the $\delta^{13}C$ therefore also oscillate.

To illustrate these cases, we run our model without astronomical forcing. For conciseness reasons, we consider only two out
290   of the four possible cases described above. We will consider the two cases for which the Ox curve crosses the unstable middle branch, corresponding to panels (a) and (d) of Figure 3. We define the parameter a_{lim} as $a_{lim} = (B_{lim1} - B_{lim2})/(O_{lim1} - O_{lim2})$. If $a_{ox} > a_{lim}$, this corresponds to the case of panel (d) of Figure 3. If $a_{ox} < a_{lim}$, this corresponds to the case depicted in panel (a) of Figure 3.

3.1.1 $a_{ox} > a_{lim}$

295   The model is run for 100 Myr with $a_{ox} = 1.5 \cdot a_{lim}$, for one specific set of model parameters. The simulations start from different initial values for the carbon and oxygen. The Ox curve intercept parameter b_{ox}, is chosen in order to follow the configuration of panel (d) of Figure 3, where the Ox curve crosses 3 times the B curve. The carbon, oxygen, organic matter burial and $\delta^{13}C$ evolution over time are displayed in Figure 4. An equilibrium is reached in less than 10 Myr for all the simulations. The equilibrium value depends on the initial conditions. This is expected as there are two stable equilibria for the
300   (C,O) system in this configuration. In the case of a different value of the parameter b_{ox}, leading to a single crossing with the B curve (case of panel (b) and (c) of Figure 3), an equilibrium would also be reached. The only difference is that the equilibrium would not depend on initial conditions, as there is only one possible equilibrium value.
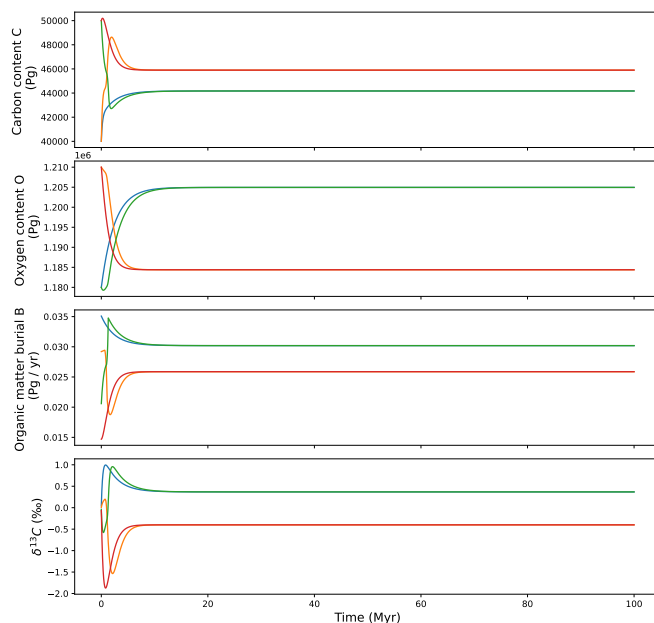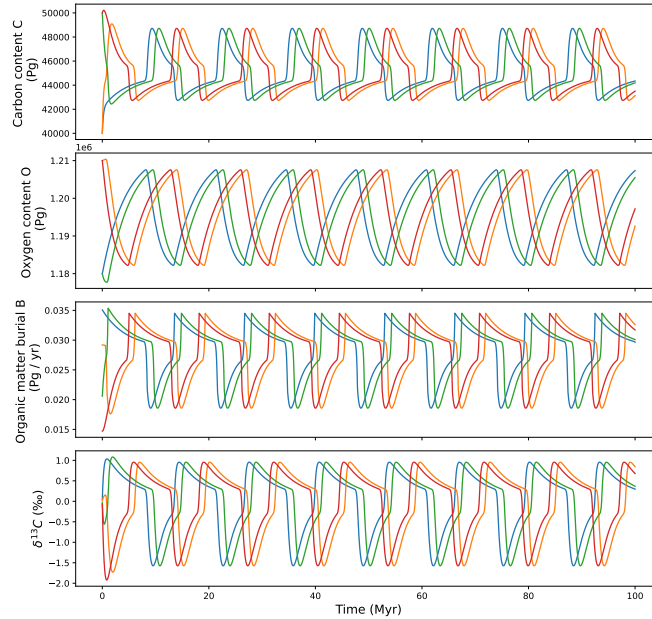
Figure 4. Modelled carbon content C, oxygen content O, organic matter burial B and $\delta^{13}C$ evolution in the case without astronomical forcing for different initial states. Case $a > a_{lim}$.

3.1.2 $a_{ox} < a_{lim}$

The model is run for 100 Myr with $a_{ox} = 0.5 \cdot a_{lim}$, for one specific set of model parameters, starting from different initial values for the carbon and oxygen. The parameter b_{ox}, is chosen in order to follow the configuration of panel (a) of Figure 3, where the Ox curve only crosses the unstable part of the B curve. The carbon, oxygen, organic matter burial and $\delta^{13}C$ evolution over time are displayed in Figure 5.

In this case, no equilibrium is reached and the system oscillates. The amplitude of the oscillations for the carbon is around 6000 PgC. The $\delta^{13}C$ oscillations have an amplitude around 2.5‰. The frequency of the oscillation is identical for the different initial conditions, and only the phase is different. The oscillations have a period of approximately 15 Myr with the parameter set used on this example. The frequency and shape of the oscillations depend on the model parameters. For example, for higher values of the δ parameter, the system would oscillate more quickly.

To sum up, we have detailed here a simple case, without astronomical forcing of the organic matter burial B. In that case, there are two possibilities for the evolution of the (C, O) system. If there is at least one stable equilibrium for the oxygen (case of panels (b), (c) and (d) of Figure 3), then the system will converge towards an equilibrium (C_{eq}, O_{eq}), and the modelled $\delta^{13}C$ will also converge towards an equilibrium. If there is no stable equilibrium for the oxygen (case of panel (a) of Figure 3), the

Figure 5. Modelled carbon content C, oxygen content O, organic matter burial B and $\delta^{13}C$ evolution in the case without astronomical forcing for different initial states. Case $a < a_{lim}$.

(C,O) system will oscillate freely, and the modelled $\delta^{13}C$ will also oscillate. However, in our model, the organic matter burial is also forced astronomically, through a dependency to eccentricity. This makes the situation more complex. When a stable equilibrium is reached in a case without astronomical forcing, the equilibrium can become unstable in the forced case, if the astronomical forcing is relatively strong (relatively high values of the a_f parameter). In this case, the astronomical forcing pushes the system away from its equilibrium towards another. This will be detailed in the third result section.

3.2 Results without oscillatory dynamics - organic matter burial not depending on surface oxygen.

In a second step, we study our model results in the case where the net organic matter burial does not depend on surface carbon and oxygen quantities, but is solely forced by the astronomical forcing : $B = B_{0cst} - a_f F(t)$, where B_{0cst} is a constant. This is close to the model of Paillard (2017). In this case we have no coupling anymore between the carbon and the oxygen cycle, and the system is linear, with an astronomical forcing.

$$\begin{cases} \frac{dC}{dt} = -\frac{1}{\tau_c}C + c_1 - 2a_f F(t) \\ \frac{dO}{dt} = -a_{ox}O + c_2 + a_f F(t) \end{cases} \tag{10}$$

with c_1 and c_2 being constants, $c_1 = 2(V_0 - B_0)$, $c_2 = B_0 - b$. As $a_{ox} > 0$ and $\frac{1}{\tau_c} > 0$ the system is stable. Without the astro-nomical forcing, it would converge towards an equilibrium. The addition of the astronomical forcing yields oscillations around

330   it.

In the following, we have run the model with the same parameters as previously, for different values of the a_f parameter. In Figure 6 the evolution of carbon, oxygen, organic carbon burial and $\delta^{13}C$ over time are displayed for $a_f = 0.01$ (green curves), $a_f = 0.03$ (orange curves) and $a_f = 0.05$ (blue curves). There are oscillations around an equilibrium value for the carbon and the $\delta^{13}C$. Changing the a_f value does not change the shape nor the frequency of the oscillations. It only changes their amplitude.

335   For the $\delta^{13}C$, the oscillation amplitude varies from around 0.5‰ for the weakest astronomical forcing considered ($a_f = 0.01$) to 2‰ for the strongest astronomical forcing considered ($a_f = 0.05$). For the carbon, the oscillation amplitude varies from around 1000 PgC to 6000 PgC.
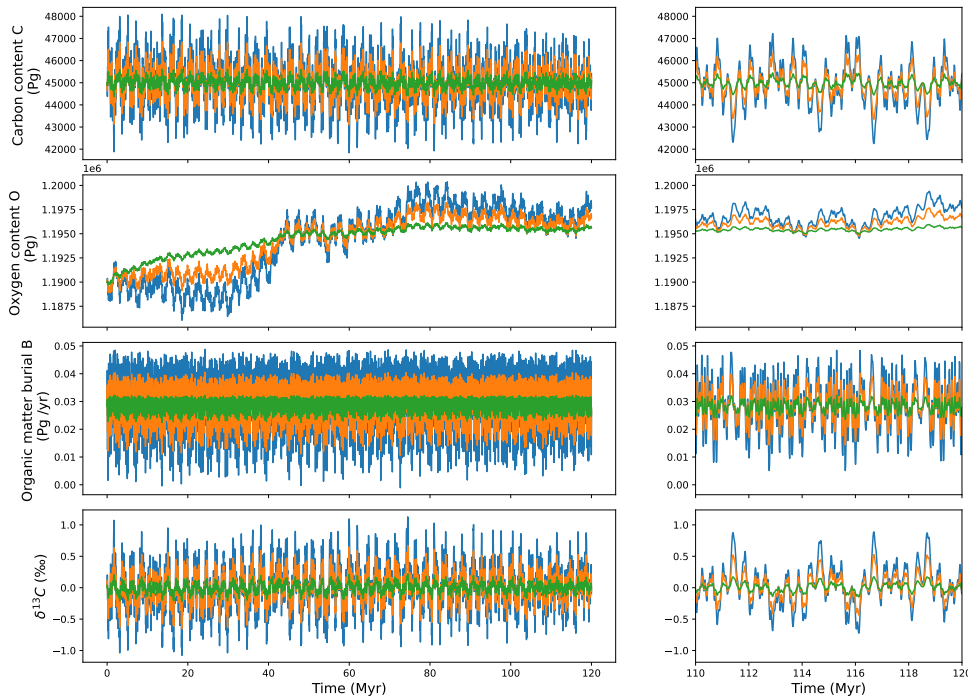
Figure 6. Modelled carbon content C, oxygen content O, organic matter burial B and $\delta^{13}C$ for different a_f values ($a_f = 0.01$ in green, $a_f = 0.03$ in orange and $a_f = 0.05$ in blue) when B_0 is a constant. The right panel is a zoom on the last 10 Myr of the simulation.

The spectral analysis of the $\delta^{13}C$ curve is shown in panel (a) of Figure 7. The dominant frequencies of the $\delta^{13}C$ oscillations are 400 kyr and 2.4 Myr. These frequencies are present in the input forcing (the eccentricity). The 400 kyr frequency is already
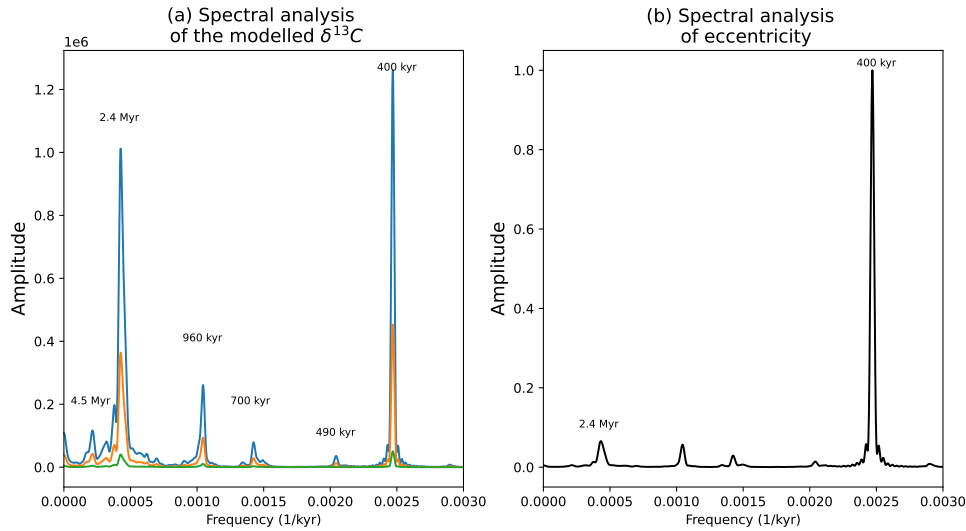
Figure 7. (a) Normalized spectral analysis of the resulting $\delta^{13}C$ for different a_f values (a_f = 0.01, 0.03 and 0.05 in green, orange and blue) when B_0 is a constant. (b) Spectral analysis of the eccentricity input forcing.

340   strong in the input forcing. However, the 2.4 Myr frequency is of low power in the eccentricity spectra, but strong in the modelled $\delta^{13}C$. The $\delta^{13}C$ spectral analysis also contains a weaker $\sim$4.5 Myr peak. This frequency is of very low amplitude in the input eccentricity forcing. As in the Paillard (2017) model, we are able to produce 400 kyr and 2.4 Myr cycles in $\delta^{13}C$ through the astronomical forcing of organic matter burial. However, as this model is linear, it is not possible to produce longer term cycles with a high amplitude, corresponding to frequencies with very low amplitude in the eccentricity spectra. A non

345   linear model is needed to produce larger periods with a strong amplitude in $\delta^{13}C$ with a simple eccentricity forcing. This is the case with our model when we add the dependency of the organic matter burial to the carbon and oxygen contents. The results for specific parameter values are discussed in the next section.

3.3   Complete model : forcing of the organic matter burial.

   Here, we use the complete form of the organic matter burial, as described in Section 2.1. The organic matter burial depends on

350   the surface carbon quantity C, the surface oxygen quantity O and the astronomical forcing : $B = B_0(C(t), O(t)) - a_f F(t)$. We perform simulations for different a_f parameter values ranging from a_f = 0 to a_f = 0.05. This corresponds to different relative importance of the astronomical forcing on the organic matter burial. The simulations are run over 120 Myr. We perform these simulations in two different cases. The first [case A] corresponds to a situation where the system oscillates freely for a_f = 0. This corresponds to panel (a) of Figure 3. The second one [case B] corresponds to a situation where the system does not

355   oscillate for a_f = 0 (presence of a stable equilibria). In our case, we have taken a situation corresponding to panel (b) of Figure 3. The evolution of $\delta^{13}C$ in these both cases is displayed in panels (a) of Figures 8 and 9. A zoom on the last 20 Myr of

simulation is provided in panels (b). The spectral analysis of the modelled $\delta^{13}C$ is displayed in panels (c). The spectral analysis were carried out with the Blackman Tuckey method implemented in the Analyseries software (Paillard et al., 1996).

In case A, the $\delta^{13}C$ oscillates freely when the system is not forced astronomically ($a_f = 0$), with an amplitude around 2‰.

360   For a relatively small influence of the astronomical forcing ($a_f = 0.01$) the shape of the large, free oscillations is still visible, and small oscillations of amplitude around 0.1‰ occur around it. However, the frequency of the free oscillations is affected by the astronomical forcing and differs from the unforced case. In case B, there are no oscillations for $a_f = 0$. For $a_f = 0.1$, oscillations similar to case A occur. In both cases, for higher values of a_f, the free oscillations are not visible anymore, and the signal is dominated by oscillations of lower period. The dominant, low period oscillations have an amplitude of around

365   2‰, and the smaller higher frequency oscillations have an amplitude of around 0.05‰. Oscillations of 400 kyr are present for all cases where the system is forced astronomically. However, their relatively low amplitude makes them hard to notice in the spectral analysis, especially for low a_f value. As the relative strength of the astronomical forcing increases (a_f increases), the power of the 400 kyr oscillations becomes stronger. The dominant period of the oscillations decreases with increasing a_f parameter.
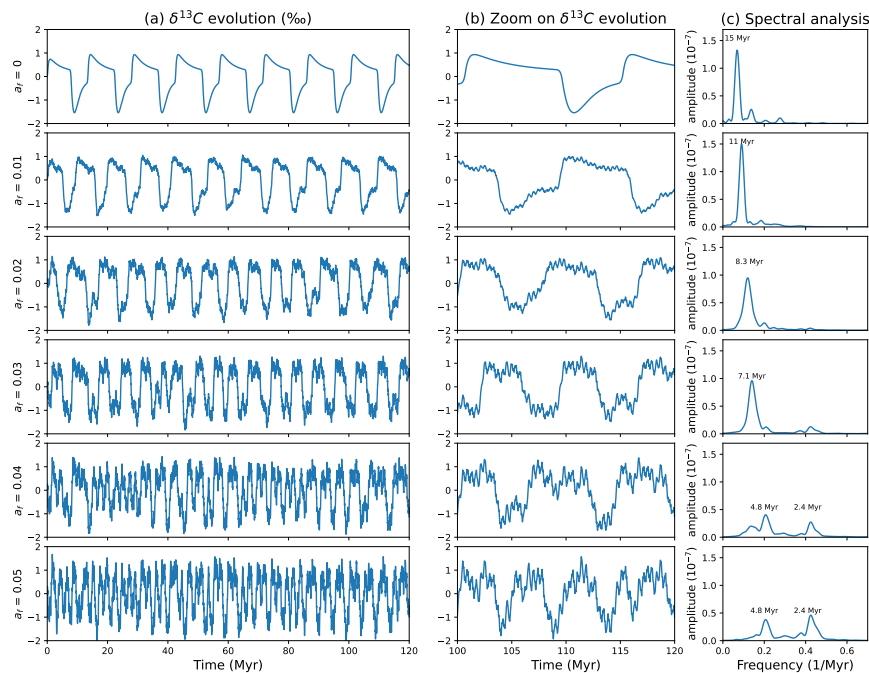

Figure 8. [case A] (a) Modelled $\delta^{13}C$ for different a_f values and $a = 0.5 \cdot a_{lim}$. (b) Zoom on the last 20 Myr of the simulation. (c) Spectral analysis of the modelled $\delta^{13}C$.
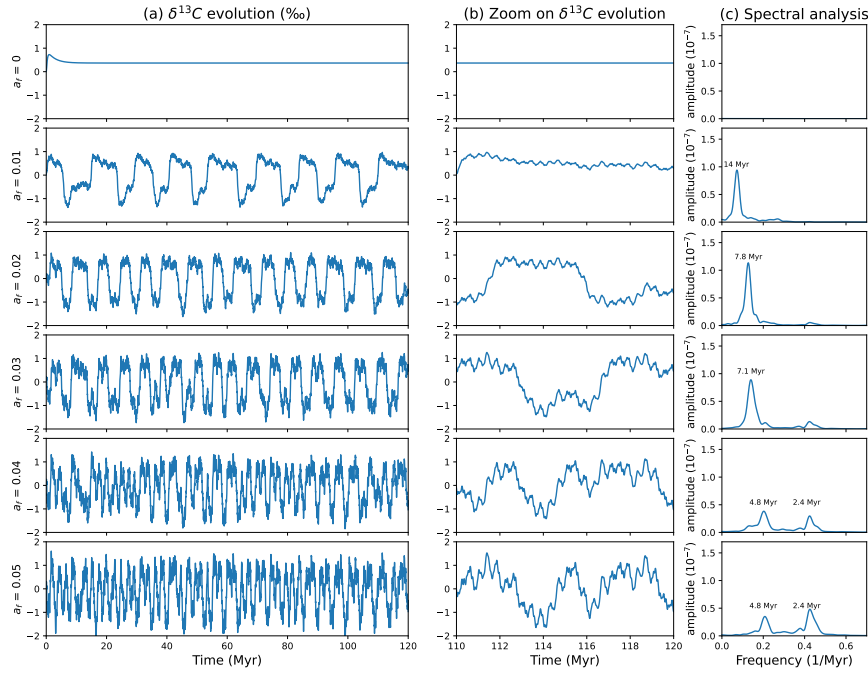
Figure 9. [case B] (a) Modelled $\delta^{13}C$ for different a_f values and $a = 1.5 \cdot a_{lim}$. (b) Zoom on the last 20 Myr of the simulation. (c) Spectral analysis of the modelled $\delta^{13}C$.

370   In both cases, the addition of the astronomical forcing changes the behaviour of the coupled system. The output signal has a dominant frequency that differs from the frequency of the unforced system. We are able to obtain oscillations on the $\delta^{13}C$ of several million years. However, one important feature to notice is that when the a_f parameter decreases, the output signal dominant period does not decrease continuously. Figure 10 represents the dominant period of the signal depending on the a_f parameter, for different parameter sets. The plot shows "steps" : there are preferential periods, meaning that for a range range

375   of a_f values, the output dominant period remains the same. The 2.4 Myr periodicity and its multiples are schematized with blue dotted lines.

For large a_f values (around 0.4 - 0.5), the dominant frequency is 2.4 Myr. Both 2.4 and 4.8 Myr periodicities are present in the spectral analysis. As the a_f parameter decreases slightly, the 4.8 Myr periodicity becomes dominant. It is particularly striking that for each parameter set, it is not possible to have a dominant frequency value between 2.4 and 4.8 Myr. The 4.8

380   Myr periodicity is the double of the 2.4 Myr periodicity of eccentricity. As the a_f parameter decreases, a period around 7 Myr becomes dominant. It is between 7.2 and 7.7 depending on the parameter set. This periodicity is not present in the eccentricity spectra. However, it corresponds to the triple of the 2.4 Myr periodicity. It is possible to obtain dominant frequencies between
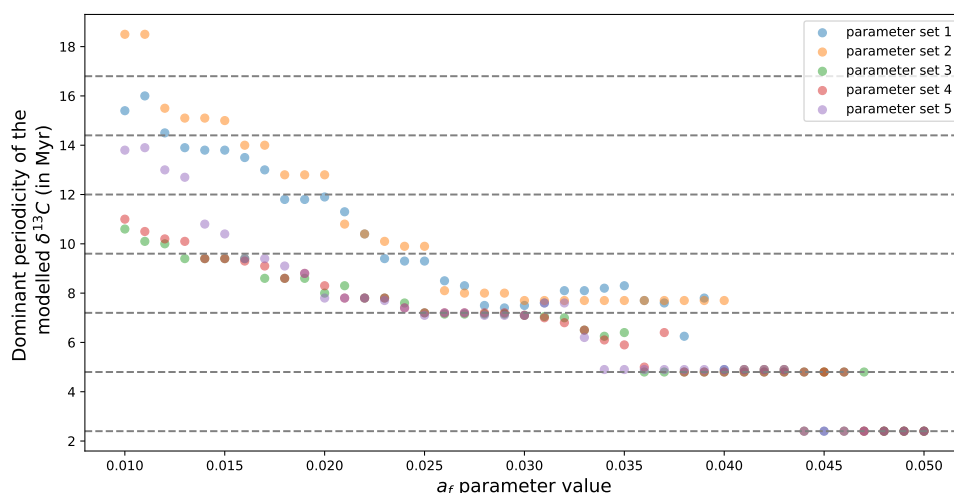
Figure 10. Dominant period of the modelled $\delta^{13}C$ as a function of the a_f value, for different parameter sets.

4.8 and 7 Myr. However, this is limited to very specific cases (specific a_f values for specific parameter values). On the contrary, the $\sim$7 Myr period is dominant for a wide range of a_f parameters, for all parameter sets (between $a_f = 0.025$ and $a_f = 0.04$ depending on the parameter set). Decreasing again the a_f parameter produces longer periods. The isolation of a preferential periodicity is not as clear as for the 2.4, 4.8 and $\sim$7 Myr frequencies, and the rise of the dominant frequency of the output signal with the a_f parameter decrease becomes more continuous. However, for each parameter set there is a small step around the fourth multiple of 2.4 Myr, $\sim$ 9.6 Myr (between 9 and 10 Myr, depending on the parameter set). The corresponding a_f interval is much smaller than in the case of the 4.8 and $\sim$7 Myr periods. As the a_f parameter decreases again, the evolution of the dominant frequencies seems to vary in a non continuous way, with preferred frequencies, but the behaviour is less clear. The presence of preferred period suggests a mechanism of frequency locking and periodicity doubling, which allows to obtain multiple of the 2.4 Myr eccentricity frequency.

As a response to a simple eccentricity forcing, our non linear model is able to produce multi-million year cycles of periods absent of the input forcing (or present with very low amplitude), most probably via a mechanism of period doubling.

However, the shape of the oscillations obtained is quite far away from the data. For each parameter set, there are values of the a_f parameter that produce $\sim$9 Myr cycles in the $\delta^{13}C$. One of them is displayed in Figure 11. For comparison, $\delta^{13}C$ from deep sea records (Zachos et al., 2001; Westerhold, 2020) are also shown. In the modelled $\delta^{13}C$, there are oscillations between high and low $\delta^{13}C$ value, and the shift between the low and high values is quite sudden. This is due to the fact that in our model the $\delta^{13}C$ has two equilibrium values, when the organic matter burial is not forced astronomically. When the astronomical forcing is added, oscillations occur around one equilibrium value, until the astronomical forcing becomes strong

	set 1	set 2	set 3	set 4	set 5
$\frac{a}{a_{lim}}$	0.5	1.5	0.2	0.5	1.5
δ	1.3e-7	1.3e-7	2e-7	2e-7	2e-7

Table 1. Value of the different parameter sets displayed in Figure 10.

enough to push the system towards the second equilibrium. 400 kyr cycles are also noticeable on top of the multi-million year oscillations. However, their strength is underestimated compared to the data.
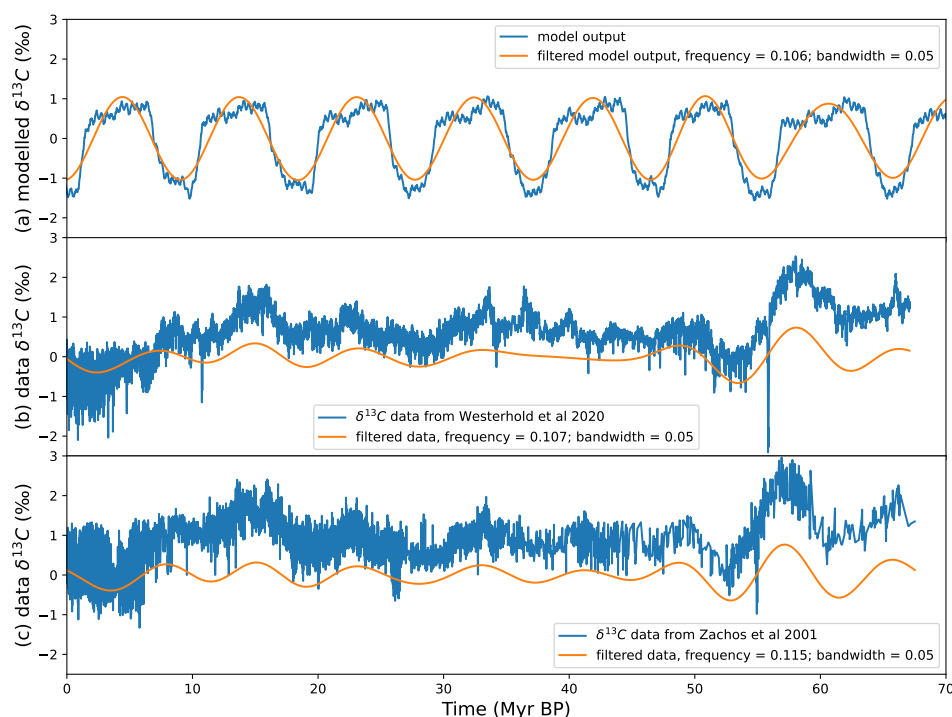
Figure 11. Comparison of (a) the modelled $\delta^{13}C$ and (b) deep sea record $\delta^{13}C$ (data are from Westerhold (2020)) in blue and filtered (frequency = 0.107; bandwidth = 0.05) in orange. The modelled $\delta^{13}C$ shown was taken among the model outputs that produces $\sim$9 Myr cyclicities.

At these timescale, many other processes not taken into account here, such as plate tectonics (Müller and Dutkiewicz, 2018), or other geochemical cycles could play a role and influence the carbon cycle. Our model is simple and excludes many pro-
405 cesses that could be of importance, and other mechanisms can be considered to produce an internal oscillatory dynamics. In this model, we have linked the carbon and oxygen cycle through the organic matter burial term. The "real" dependency of

Earth System
Dynamics
Discussions

Open Access

EGU

the net organic carbon burial B to the surface carbon C and thus climate is probably much more complicated than the shape
envisaged here. However, the results obtained are generic, and multiple equilibria and self-sustained oscillations (without any
external forcing like eccentricity) could be obtained in the Earth system with a different shape of B corresponding to different

410 mechanisms. One of the conditions to allow for multiple equilibria to exist is to have a non monotonic dependency of B(C).
That B(C) has the same shape as the one assumed in this study is highly unlikely, but the fact that B varies in a non monotonic
way with climate and thus the carbon content C is highly probable, due to the variety of processes involved, that might be
favored for certain climate and thus lower or higher carbon values. One could also imagine to obtain more complex oscillations
involving the sulfur cycle. Oxidation of sulfide minerals produces sulfuric acid, which can react with carbonate minerals and

415 thus release CO_2 (Torres et al., 2014). And sulfide oxidation also affects the oxygen content. Here, we have based the oscilla-
tions on the (C,O) elements, but other mechanisms could certainly be considered.

4   Conclusions

Multi-million year oscillations are present in the $\delta^{13}C$ records throughout the Cenozoic and part of the Mesozoic. It has been

420 suggested that these variations could be related to astronomical forcing of organic matter burial fluxes. However, no modelling
study has been able to perform such long oscillations through astronomical forcing of organic matter fluxes. Here, we have
proposed a mechanism that could explain the presence of multi-million year cycles in the $\delta^{13}C$ record, and their stability over
time, as a result of preferential periodicity locking to multiples of astronomical forcing periods. A simple, linear astronomical
forcing cannot alone produce multi-million year cycles longer than 2.4 Myr with a strong amplitude, but the presence of

425 multiple equilibria in our model allows to extract longer periods. Our result show that astronomical forcing, superimposed to
internal oscillations of the climate system (like here with carbon and oxygen) is a way to obtain very long term cycles on $\delta^{13}C$,
with periodicities that are not directly present in the initial astronomical forcing.

Earth System
Dynamics

Discussions

References

Archer, D., Kheshgi, H., and Maier-Reimer, E.: Multiple timescales for neutralization of fossil fuel CO2, Geophysical Research Letters, 24, 405–408, https://doi.org/https://doi.org/10.1029/97GL00168, 1997.

435 Baroni, I. R., Palastanga, V., and Slomp, C. P.: Enhanced Organic Carbon Burial in Sediments of Oxygen Minimum Zones Upon Ocean Deoxygenation, Frontiers in Marine Science, 6, https://doi.org/10.3389/fmars.2019.00839, 2020.

Bergman, N. M., Lenton, T. M., and Watson, A. J.: COPSE: A new model of biogeochemical cycling over Phanerozoic time, American Journal of Science, 304, 397–437, https://doi.org/10.2475/ajs.304.5.397, 2004.

Berner, R.: Modeling atmospheric O2 over Phanerozoic time, Geochimica et Cosmochimica Acta, 65, 685–694, 440 https://doi.org/https://doi.org/10.1016/S0016-7037(00)00572-X, 2001.

Berner, R. A. and Canfield, D. E.: A new model for atmospheric oxygen over Phanerozoic time, American Journal of Science, 289, 333–361, https://doi.org/10.2475/ajs.289.4.333, 1989.

Billups, K., Pälike, H., Channell, J., Zachos, J., and Shackleton, N.: Astronomic calibration of the late Oligocene through early Miocene geomagnetic polarity time scale, Earth and Planetary Science Letters, 224, 33–44, https://doi.org/https://doi.org/10.1016/j.epsl.2004.05.004, 445 2004.

Bolton, E. W., Berner, R. A., and Petsch, S. T.: The Weathering of Sedimentary Organic Matter as a Control on Atmospheric O2: II. Theoretical Modeling, American Journal of Science, 306, 575–615, https://doi.org/10.2475/08.2006.01, 2006.

Bopp, L., Le Quéré, C., Heimann, M., Manning, A. C., and Monfray, P.: Climate-induced oceanic oxygen fluxes: Implications for the contemporary carbon budget, Global Biogeochemical Cycles, 16, 6–1–6–13, https://doi.org/https://doi.org/10.1029/2001GB001445, 2002.

450 Boulila, S., Galbrun, B., Laskar, J., and Pälike, H.: A ∼9myr cycle in Cenozoic $\delta^{13}C$ record and long-term orbital eccentricity modulation: Is there a link?, Earth and Planetary Science Letters, 317-318, 273–281, https://doi.org/https://doi.org/10.1016/j.epsl.2011.11.017, 2012.

Burton, M. R., Sawyer, G. M., and Granieri, D.: Deep Carbon Emissions from Volcanoes, Reviews in Mineralogy and Geochemistry, 75, 323–354, https://doi.org/10.2138/rmg.2013.75.11, 2013.

Canfield, D.: THE EARLY HISTORY OF ATMOSPHERIC OXYGEN: Homage to Robert M. Garrels, Annual Review of Earth and Planetary 455 Sciences, 33, 1–36, https://doi.org/10.1146/annurev.earth.33.092203.122711, 2005.

Chang, S. and Berner, R. A.: Coal weathering and the geochemical carbon cycle, Geochimica et Cosmochimica Acta, 63, 3301–3310, https://doi.org/https://doi.org/10.1016/S0016-7037(99)00252-5, 1999.

Ciais, P., Sabine, C., Bala, G., L. Bopp, V. B., Canadell, J., Chhabra, A., DeFries, R., Galloway, J., Heimann, M., Jones, C., Quéré, C. L., Myneni, R., Piao, S., and Thornton, P.: Carbon and Other Biogeochemical Cycles. In : Climate Change 2013: The Physical Science 460 Basis. Contribution of Working Group I to the Fifth Assessment Report of the Intergovernmental Panel on Climate Change, Cambridge University Press, Cambridge, United Kingdom and New York, NY, USA, 2013.

de Boer, B., Lourens, L., and van de Wal, R.: Persistent 400,000-year variability of Antarctic ice volume and the carbon cycle is revealed throughout the Plio-Pleistocene., Nat Commun, 5, 299, https://doi.org/10.1038/ncomms3999, 2014.

Hedges, J. I. and Keil, R. G.: Sedimentary organic matter preservation: an assessment and speculative synthesis, Marine Chemistry, 49, 465 81–115, https://doi.org/https://doi.org/10.1016/0304-4203(95)00008-F, 1995.

Hemingway, J. D., Hilton, R. G., Hovius, N., Eglinton, T. I., Haghipour, N., Wacker, L., Chen, M.-C., and Galy, V. V.: Microbial oxidation of lithospheric organic carbon in rapidly eroding tropical mountain soils, Science, 360, 209–212, https://doi.org/10.1126/science.aao6463, 2018.

Earth System
Dynamics
Discussions

Hilton, R. G.: Climate regulates the erosional carbon export from the terrestrial biosphere, Geomorphology, 277, 118–132,
470   https://doi.org/https://doi.org/10.1016/j.geomorph.2016.03.028, connectivity in Geomorphology from Binghamton 2016, 2017.

Hilton, R. G. and West, A. J.: Mountains, erosion and the carbon cycle, Nature Reviews Earth Environment, 1, 284–299,
       https://doi.org/10.1038/s43017-020-0058-6, 2020.

Hilton, R. G., Gaillardet, J., Calmels, D., and Birck, J.-L.: Geological respiration of a mountain belt revealed by the trace element rhenium,
       Earth and Planetary Science Letters, 403, 27–36, https://doi.org/https://doi.org/10.1016/j.epsl.2014.06.021, 2014.

475   Jessen, G. L., Lichtschlag, A., Ramette, A., Pantoja, S., Rossel, P. E., Schubert, C. J., Struck, U., and Boetius, A.: Hypoxia causes preser-
       vation of labile organic matter and changes seafloor microbial community composition (Black Sea), Science Advances, 3, e1601 897,
       https://doi.org/10.1126/sciadv.1601897, 2017.

Kocken, I. J., Cramwinckel, M. J., Zeebe, R. E., Middelburg, J. J., and Sluijs, A.: The 405 kyr and 2.4 Myr eccentricity components in
       Cenozoic carbon isotope records, Climate of the Past, 15, 91–104, https://doi.org/10.5194/cp-15-91-2019, 2019.

480   Kurtz, A. C., Kump, L. R., Arthur, M. A., Zachos, J. C., and Paytan, A.: Early Cenozoic decoupling of the global carbon and sulfur cycles,
       Paleoceanography, 18, https://doi.org/https://doi.org/10.1029/2003PA000908, 2003.

Laskar, J., Robutel, P., Joutel, F., Gastineau, M., Correia, A. C. M., and Levrard, B.: A long-term numerical solution for the insolation
       quantities of the Earth, A&A, 428, 261–285, https://doi.org/10.1051/0004-6361:20041335, 2004.

Laskar, J., Fienga, A., Gastineau, M., and Manche, H.: La2010: a new orbital solution for the long-term motion of the Earth, A&A, 532,
485   A89, https://doi.org/10.1051/0004-6361/201116836, 2011.

Lauretano, V., Littler, K., Polling, M., Zachos, J. C., and Lourens, L. J.: Frequency, magnitude and character of hyperthermal events at the
       onset of the Early Eocene Climatic Optimum, Climate of the Past, 11, 1313–1324, https://doi.org/10.5194/cp-11-1313-2015, 2015.

Laurin, J., Meyers, S. R., Uličný, D., Jarvis, I., and Sageman, B. B.: Axial obliquity control on the greenhouse carbon budget through middle-
       to high-latitude reservoirs, Paleoceanography, 30, 133–149, https://doi.org/https://doi.org/10.1002/2014PA002736, 2015.

490   Liebrand, D., Beddow, H. M., Lourens, L. J., Pälike, H., Raffi, I., Bohaty, S. M., Hilgen, F. J., Saes, M. J., Wilson, P. A., van Dijk, A. E.,
       Hodell, D. A., Kroon, D., Huck, C. E., and Batenburg, S. J.: Cyclostratigraphy and eccentricity tuning of the early Oligocene through
       early Miocene (30.1–17.1 Ma): Cibicides mundulus stable oxygen and carbon isotope records from Walvis Ridge Site 1264, Earth and
       Planetary Science Letters, 450, 392–405, https://doi.org/https://doi.org/10.1016/j.epsl.2016.06.007, 2016.

Ludwig, W., Probst, J.-L., and Kempe, S.: Predicting the oceanic input of organic carbon by continental erosion, Global Biogeochemical
495   Cycles, 10, 23–41, https://doi.org/https://doi.org/10.1029/95GB02925, 1996.

Martinez, M. and Dera, G.: Orbital pacing of carbon fluxes by a ˜9-My eccentricity cycle during the Mesozoic, Proceedings of the National
       Academy of Sciences, 112, 12 604–12 609, https://doi.org/10.1073/pnas.1419946112, 2015.

Meybeck, M.: Carbon, nitrogen, and phosphorus transport by world rivers, American Journal of Science, 282, 401–450,
       https://doi.org/10.2475/ajs.282.4.401, 1982.

500   Müller, R. D. and Dutkiewicz, A.: Oceanic crustal carbon cycle drives 26-million-year atmospheric carbon dioxide periodicities, Science
       Advances, 4, eaaq0500, https://doi.org/10.1126/sciadv.aaq0500, 2018.

Niemeyer, D., Kemena, T. P., Meissner, K. J., and Oschlies, A.: A model study of warming-induced phosphorus–oxygen feedbacks in open-
       ocean oxygen minimum zones on millennial timescales, Earth System Dynamics, 8, 357–367, https://doi.org/10.5194/esd-8-357-2017,
       2017.

505   Paillard, D.: The Plio-Pleistocene climatic evolution as a consequence of orbital forcing on the carbon cycle, Climate of the Past, 13, 1259–
       1267, https://doi.org/10.5194/cp-13-1259-2017, 2017.

Paillard, D., Labeyrie, L., and Yiou, P.: Macintosh Program performs time-series analysis, Eos, Transactions, AGU, 77, 379–379, https://doi.org/10.1029/96EO00259, 1996.

Petsch, S., Edwards, K., and Eglinton, T.: Microbial transformations of organic matter in black shales and im-
510   plications for global biogeochemical cycles, Palaeogeography, Palaeoclimatology, Palaeoecology, 219, 157–170, https://doi.org/https://doi.org/10.1016/j.palaeo.2004.10.019, geobiology: Objectives, Concept, Perspectives, 2005.

Pälike, H., Norris, R. D., Herrle, J. O., Wilson, P. A., Coxall, H. K., Lear, C. H., Shackleton, N. J., Tripati, A. K., and Wade, B. S.: The Heartbeat of the Oligocene Climate System, Science, 314, 1894–1898, https://doi.org/10.1126/science.1133822, 2006.

Russon, T., Paillard, D., and Elliot, M.: Potential origins of 400–500 kyr periodicities in the ocean carbon cycle: A box model approach,
515   Global Biogeochemical Cycles, 24, https://doi.org/https://doi.org/10.1029/2009GB003586, 2010.

Smith, J. C., Galy, A., Hovius, N., Tye, A. M., Turowski, J. M., and Schleppi, P.: Runoff-driven export of par-
ticulate organic carbon from soil in temperate forested uplands, Earth and Planetary Science Letters, 365, 198–208, https://doi.org/https://doi.org/10.1016/j.epsl.2013.01.027, 2013.

Sproson, A. D.: Pacing of the latest Ordovician and Silurian carbon cycle by a 4.5 Myr orbital cycle, Palaeogeography, Palaeoclimatology,
520   Palaeoecology, 540, 109 543, https://doi.org/https://doi.org/10.1016/j.palaeo.2019.109543, 2020.

Sprovieri, M., Sabatino, N., Pelosi, N., Batenburg, S. J., Coccioni, R., Iavarone, M., and Mazzola, S.: Late Cretaceous orbitally-paced carbon isotope stratigraphy from the Bottaccione Gorge (Italy), Palaeogeography, Palaeoclimatology, Palaeoecology, 379-380, 81–94, https://doi.org/https://doi.org/10.1016/j.palaeo.2013.04.006, 2013.

Stolper, D. A., Bender, M. L., Dreyfus, G. B., Yan, Y., and Higgins, J. A.: A Pleistocene ice core record of atmospheric O_2 concentrations,
525   Science, 353, 1427–1430, https://doi.org/10.1126/science.aaf5445, 2016.

Stramma, L., Johnson, G. C., Sprintall, J., and Mohrholz, V.: Expanding Oxygen-Minimum Zones in the Tropical Oceans, Science, 320, 655–658, https://doi.org/10.1126/science.1153847, 2008.

Stramma, L., Schmidtko, S., Levin, L. A., and Johnson, G. C.: Ocean oxygen minima expansions and their biological impacts, Deep Sea Research Part I: Oceanographic Research Papers, 57, 587–595, https://doi.org/https://doi.org/10.1016/j.dsr.2010.01.005, 2010.

530   Torres, M., West, A., and Li, G.: Sulphide oxidation and carbonate dissolution as a source of CO2 over geological timescales., Nature, 507, 346–349, https://doi.org/10.1038/nature03814, 2014.

Wang, P., Tian, J., and Lourens, L. J.: Obscuring of long eccentricity cyclicity in Pleistocene oceanic carbon isotope records, Earth and Planetary Science Letters, 290, 319–330, https://doi.org/https://doi.org/10.1016/j.epsl.2009.12.028, 2010.

Westerhold, T.: Cenozoic global reference benthic carbon and oxygen isotope dataset (CENOGRID),
535   https://doi.org/10.1594/PANGAEA.917503, 2020.

Westerhold, T., Röhl, U., Donner, B., McCarren, H. K., and Zachos, J. C.: A complete high-resolution Paleocene benthic stable isotope record for the central Pacific (ODP Site 1209), Paleoceanography, 26, https://doi.org/https://doi.org/10.1029/2010PA002092, 2011.

Zachos, J., Pagani, M., Sloan, L., Thomas, E., and Billups, K.: Trends, Rhythms, and Aberrations in Global Climate 65 Ma to Present, Science, 292, 686–693, https://doi.org/10.1126/science.1059412, 2001.